Advanced Steel Construction – Vol. 20 No. 2 (2024) 149–159
DOI:10.18057/IJASC.2024.20.2.7
(Special Issue: *11st International Conference on Advances in Steel Structures, ICASS'2023, Kuching, Sarawak, Malaysia*)

BIFURCATION BUCKLING LOAD OF STEEL ANGLE WITH RANDOM CORROSION DAMAGE

Liang Chen [1], Jing-Zhou Zhang [2, *], Si-Wei Liu [1] and Zhi-Wei Yu [2]

[1] *Department of Civil and Environmental Engineering, The Hong Kong Polytechnic University, Hung Hom, Kowloon, Hong Kong, China*
[2] *School of Civil Engineering, Guangzhou University, Guangzhou, China*
[*] *(Corresponding author: E-mail: 205352@gzhu.edu.cn)*

ABSTRACT

This paper numerically studies the bifurcation buckling load of steel angle members affected by random corrosion pits. Six million Monte Carlo simulations are conducted, in which the effects of member length, section type, area loss ratio, and corrosion depth on the bifurcation buckling load of steel angles are considered. The key statistical characteristics of the reduction factors of buckling load for steel angles are analyzed. A probability-based relationship between the reduction factor of buckling load and the area loss ratio of steel angles is also proposed for the practical design. It is found that corrosion can potentially change the buckling mode of steel angle members from flexural buckling to torsional buckling. When the member length is small, the bifurcation buckling load of the steel angle is significantly affected by the corrosion depth. However, with the increase in member length, the effect of corrosion depth tends to decrease. The reduction factors of the buckling load of steel angles follow a normal distribution. A larger area loss ratio will result in a larger standard deviation of the reduction factors. For steel angles with the same area loss ratio, the mean values of the reduction factors of different section types are very close.

ARTICLE HISTORY

Received: 8 April 2024
Revised: 16 May 2024
Accepted: 5 June 2024

KEYWORDS

Buckling load;
Steel angle;
Random corrosion;
Monte Carlo simulation;
Area loss ratio;
Corrosion depth

1. Introduction

Steel structures will inevitably be corroded due to exposure to an aggressive environment. Corrosion weakens the strength and ductility of steel material and, meanwhile, reduces the sectional area of steel components, which results in the deterioration of steel structures. The deterioration process of steel structures is highly random and unpredictable, which reduces the safety and reliability of the structure by a great extent [1].

Currently, a considerable amount of literature can be found on the corrosion effects of steel structures. The research objects of these studies mainly include: steel material [2-5], plate [6-9], rebar [10-14], beam [15-17], column [18-24], joint [25-28], pipeline [29-32], and structure [33-37]. Zhao *et al.* [2] numerically studied the mechanical properties of Q345 steel with random corrosion pits. The reduction of the nominal ultimate strength of corroded Q345 steel was affected by both the mass loss ratio and corrosion depth. Wang *et al*. [9] studied the compression behavior of corroded steel plates, considering different pit shapes, distributions, and depths. It was found that corrosion pits will not only reduce the ultimate strength of steel plate but also change its failure mode. Zhang *et al*. [11] studied the corrosion evolution process in rebar and found that the corrosion depth followed the Poisson distribution, and the longitudinal nonuniformity factor (the ratio of average section area to the minimum one) followed the Gumbel distribution. Chen *et al*. [16] proposed an efficient algorithm to compute the elastic buckling load/moment of steel members with random corrosion pits. The results show that corrosion reduces the axial-torsional buckling load of the member with greater extent than the lateral-torsional buckling moment and flexural buckling load. Hisazumi and Kanno [24] investigated the compression behavior of corroded angle-section and channel-section steel members. The ultimate capacity of the member can be better described by the minimum section area of the member. Wang *et al*. [27] studied the cyclic performance of welded beam-to-column joints in a salt spray environment with 5% mass fraction of *NaCl* solution. When the corrosion time reached 18 months, the yield moment, ultimate moment, ultimate rotation, and total energy dissipation were decreased by 28.2%, 32.1%, 49.4%, and 70.8%, respectively. In the study by Huang *et al*. [37], the fatigue reliability of a ship welded structure with random corrosion was evaluated. Altogether 151,527,600 random corrosion pits were generated in the numerical model. The relationship between the fatigue damage of the structure and corrosion deterioration was further quantified.

From the above studies, a considerable number of conclusions have been reached with great practical value. However, there are still some shortcomings existing in current studies. First, the section types of these members are mainly I-shaped [15-18] and circular-shaped [19, 20, 30, 32]. Relevant studies on angle members are scarce. Considering that the angle section is not symmetric, the mechanism of corrosion effect on the buckling load, as well as the failure mode of the corroded member, should be more complicated compared with the members with symmetric sections [24]. Therefore, a systematic understanding of the buckling load of corroded steel angle members is necessary. Second, to sufficiently capture the random nature of corrosion pits, using commercial finite element analysis software is cumbersome and time-consuming to ensure a sufficient number of Monte Carlo simulations. Therefore, an efficient algorithm is required to study the effect of random corrosion pits on steel members.

This paper numerically studies the bifurcation buckling load of steel angle members with random corrosion pits. Six million Monte Carlo simulations are conducted, in which the effects of member length, section type, area loss ratio, and corrosion depth on the bifurcation buckling load of steel angles are studied. The key statistical characteristics of the reduction factors of buckling load for steel angles are analyzed. A probability-based relationship between the reduction factor of buckling load and the area loss ratio of steel angles is also proposed. This paper is divided into seven sections. After this Introduction, analytical calculations of the buckling loads for steel angle members are introduced in Section 2. The simulation of random corrosion pits is illustrated in Section 3. A flowchart to compute the buckling load of steel angles with random corrosion pits is given in Section 4. Verification of the proposed algorithm is conducted in Section 5. Parametric studies of the buckling loads of corroded steel angle members are conducted in Section 6. The main findings and conclusions from this paper are summarized in Section 7.

2. Bifurcation buckling load

For steel angle members in compression, typical buckling modes are shown in Fig. 1 [38, 39]. Note that the local plate buckling mode is not considered in this study. The section has the smallest and largest bending rigidity about *V*- and *W*-axis, respectively.

The bifurcation buckling load of the compressed steel members with simply supported boundary conditions can be obtained by solving the following equation [40, 41]:

$$P_{cr}^3(r^2 - v_s^2 - w_s^2) - P_{cr}^2[(P_v + P_w + P_r)r^2 - P_w v_s^2 - P_v w_s^2] + P_{cr} r^2 (P_v P_w + P_w P_r + P_r P_v) - (P_v P_w P_r r^2) = 0 \quad (1)$$

wherein P_{cr} is the bifurcation buckling load of the steel member in compression. P_v and P_w are the flexural buckling load of the member about the *V*- and *W*-axis, respectively. P_r is the torsional buckling load of the member. P_v, P_w and P_r are given by [41]:

$$P_v = \frac{\pi^2 E I_v}{L^2} \quad (2)$$

$$P_w = \frac{\pi^2 E I_w}{L^2} \tag{3}$$

$$P_r = \frac{GJ + \pi^2 E I_\omega / L^2}{w_s^2 + v_s^2 + (I_w + I_v)/A_0} \tag{4}$$

wherein E and G are the Young's modulus and shear modulus of steel, respectively. A_0 is the section area. L is the member length. J is the section torsional rigidity. I_v and I_w are the section moment of inertia about V- and W-axis, respectively. I_ω is the section warping constant. w_s and v_s are the w- and v-coordinate of section shear center, respectively. Detailed calculations of these parameters can be found in Ref. [41].

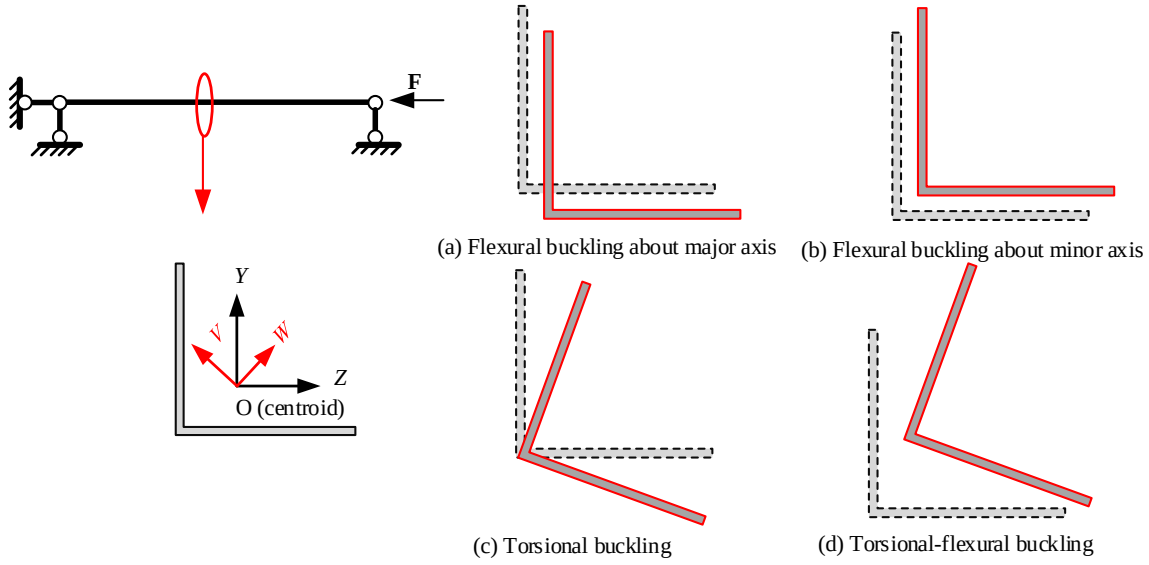

Fig. 1 Typical buckling modes of steel angle member in compression

3. Simulation of corrosion pits

Fig. 2 shows the simulation of random corrosion pits on the section. H and W represent the length of the two legs and t is the thickness of the intact section. The section is initially meshed into several line segments, with mesh size of l_s=1 mm. t_d is the corrosion depth, and the corrosion damage is considered by reducing the segment thickness by the value of t_d. For simplicity, the thickness of each damaged segment is assumed to be identical.

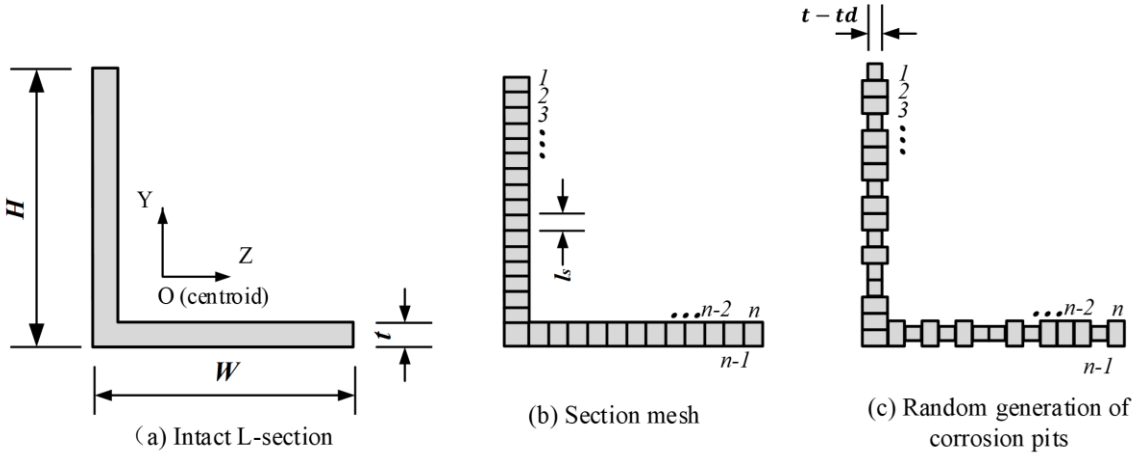

Fig. 2 Modeling of random corrosion pits

The total number of damaged segments n_d can be computed by:

$$n_d = \frac{A_0 \eta_A}{l_s t_d} = \frac{t N_0 \eta_A}{t_d} \tag{5}$$

wherein A_0 and η_A are the section area and section area loss ratio, respectively. N_0 is the total segment number (including both the intact and damaged segments).

In Equation (5), once the corrosion depth and section area loss ratio is known, the total number of damaged segments at the section can be determined. In this study, the considered values for the corrosion depth and section area loss ratio are 0.2-0.9 times the section thickness and 10%-50%, respectively. The details are summarized in Table 1. After the total number of damaged segments is determined, the corrosion pits are randomly generated at different locations on the section by Monte Carlo simulation. Then the section parameters in Equations. (2)-(4) can be computed and the bifurcation buckling load of the member P_{cr} in Equation (1) can be solved.

Table 1
Considered values of corrosion depth and section area loss ratio

Area loss ratio η_A	Corrosion depth t_d
10%	0.2t, 0.3t, 0.4t, 0.5t, 0.6t, 0.7t, 0.8t, 0.9t
20%	0.3t, 0.4t, 0.5t, 0.6t, 0.7t, 0.8t, 0.9t
30%	0.4t, 0.5t, 0.6t, 0.7t, 0.8t, 0.9t
40%	0.5t, 0.6t, 0.7t, 0.8t, 0.9t
50%	0.6t, 0.7t, 0.8t, 0.9t

4. Flowchart

The flowchart for calculating the bifurcation buckling load of a corroded steel angle member is illustrated in Fig. 3. The section area loss ratio and corrosion depth are firstly assigned. Then the total number of corrosion pits is calculated, and the corrosion pits are generated randomly at the section. Subsequently, section key parameters J, I_v, I_w, w_s, v_s, and I_o in Equations (2)-(4) are calculated, and the bifurcation buckling load of the member can be determined. The sample size of the Monte Carlo simulation is set to be 5000 for a given total number of corrosion pits. The reasonability of this value will be verified in Section 6. All the values of the section area loss ratio and corrosion depth are traversed by the algorithm. The bifurcation buckling loads of the members in each Monte Carlo simulation are exported.

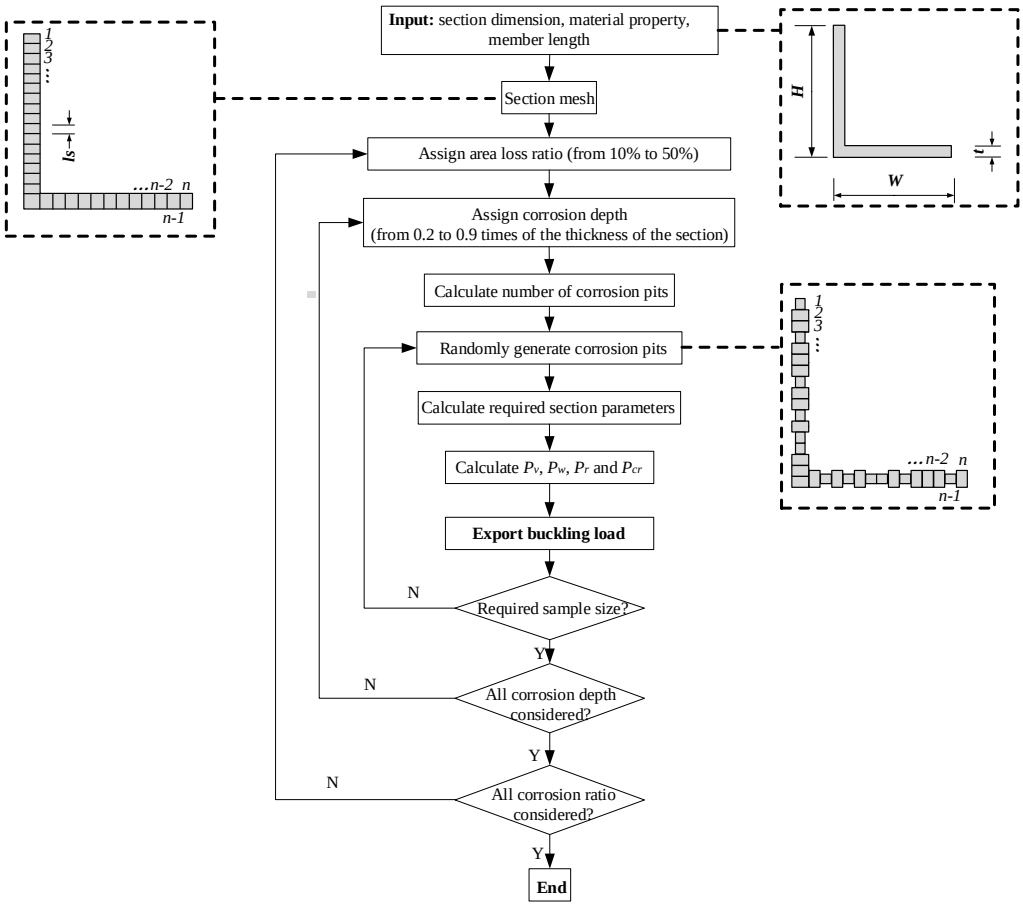

Fig. 3 Flowchart for determining the buckling loads of steel angle member with random corrosion pits

5. Verification

The software MASTAN2 [42] is used to verify the reliability and accuracy of the proposed algorithm. MASTAN2 is an educational structural analysis software. The bifurcation buckling loads from MASTAN2 and proposed algorithm for simply supported angle member are compared. Ten values of member length are considered, from 0.5 m to 5 m, with an interval of 0.5 m. Four section types are studied, as shown in Fig. 4. Section A is an intact section. Sections B, C and D are corroded sections, with area loss ratio of 10%. The comparisons of the buckling load from MASTAN2 and proposed algorithm are shown in Fig. 5. The error is calculated by:

$$\text{Error (\%)} = \frac{P_{cr-proposed} - P_{cr-MASTAN2}}{P_{cr-MASTAN2}} \tag{6}$$

wherein $P_{cr\text{-}proposed}$ and $P_{cr\text{-}MASTAN2}$ are the bifurcation buckling load from proposed algorithm and MASTAN2, respectively.

It can be seen that satisfactory agreements have been achieved between the results from the proposed algorithm and MASTAN2. The errors of the proposed algorithm are generally within 2%. The largest error of 4% occurs for section D when the member length is 1 m. By comparing Fig. 5(b), (c), and (d), it is also found that the buckling loads of the member with sections B, C, and D are very close. For example, for the member length of 2.5 m, 3m, and 3.5 m, the buckling loads of the member with sections B, C, and D are about 200 kN, 150 kN, and 100 kN, respectively.

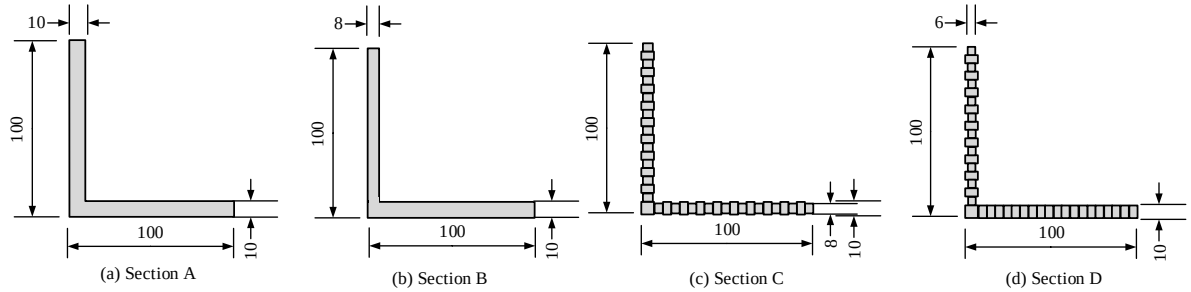

Fig. 4 Sections selected for verification of the algorithm

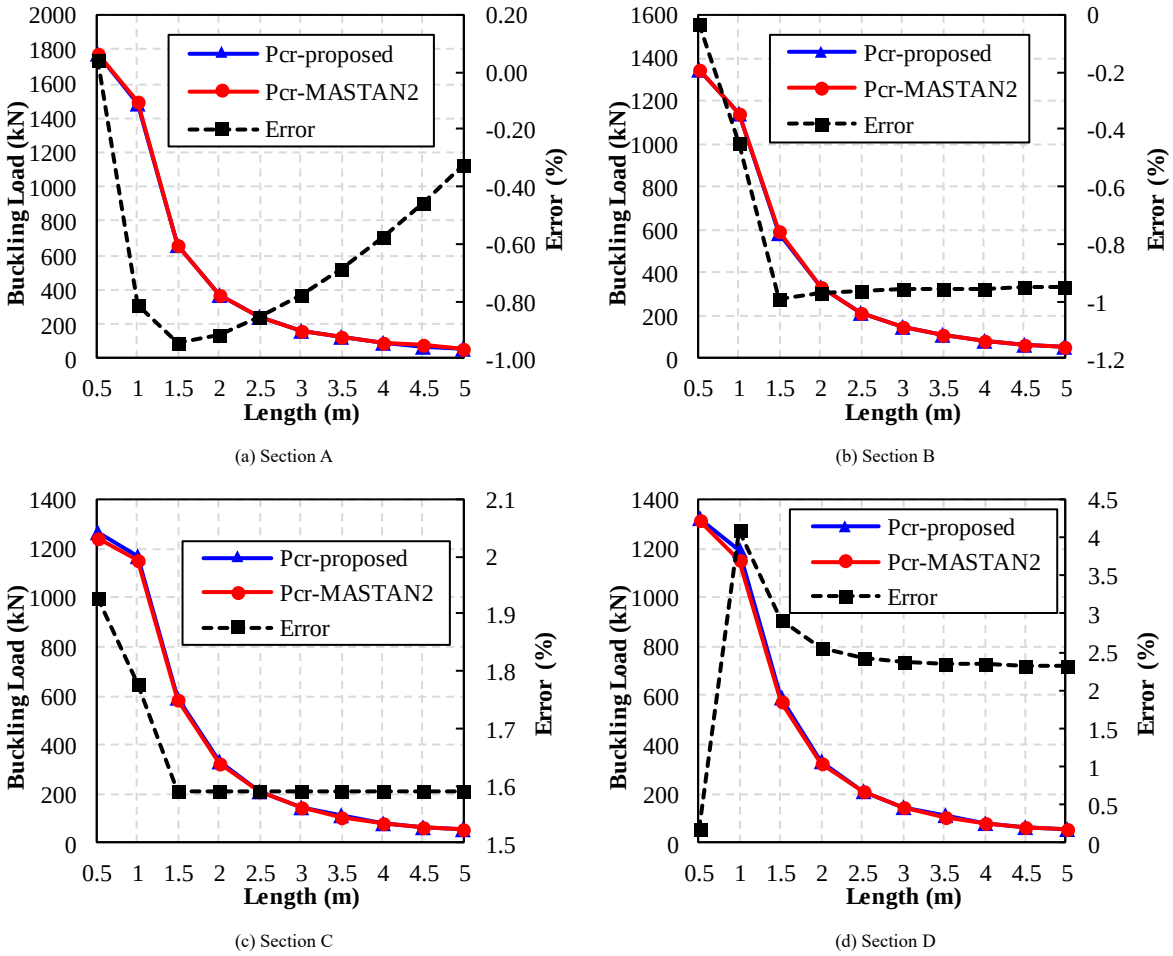

(a) Section A (b) Section B

(c) Section C (d) Section D

Fig. 5 Validation of the proposed algorithm

6. Bifurcation buckling load assessment

A total of six million Monte Carlo simulations are conducted to study the bifurcation buckling load of corroded steel angles. The considered variables include the member length, section dimension, area loss ratio, and corrosion depth. The values of section area loss ratio and corrosion depth are presented in Table 1. Five sections are selected from the code of Structural Steel Equal and Unequal Leg Angles [43], three of which are equal leg angles, and two are unequal leg angles. For each section, eight values of member length are considered. The details are given in Table 2. A convergence study is firstly conducted to determine a reasonable sample size of Monte Carlo simulation in each corrosion scenario, considering both the efficiency and accuracy of the algorithm. After computation, the buckling curves of corroded steel angle members are exhibited. The effects of the area loss ratio and corrosion depth on the buckling load of steel angle are analyzed. Moreover, the relationship between the reduction factor and the area loss ratio of the corroded steel angle is studied.

Table 2
Details of section dimension and member length

Section (mm)	I_y (cm^4)	I_z (cm^4)	i_y (cm)	i_z (cm)	Member length (m)
L100×100×12	207	207	3.02	3.02	0.5, 1, 1.5, 2, 2.5, 3, 3.5, 4
L150×150×18	1050	1050	4.54	4.54	0.75, 1.5, 2.25, 3, 3.75, 4.5, 5.25, 6
L200×200×24	3330	3330	6.06	6.06	1, 2, 3, 4, 5, 6, 7, 8
L150×100×12	233	651	2.85	4.76	0.5, 1, 1.5, 2, 2.5, 3, 3.5, 4
L200×100×12	247	1440	2.67	6.43	0.5, 1, 1.5, 2, 2.5, 3, 3.5, 4

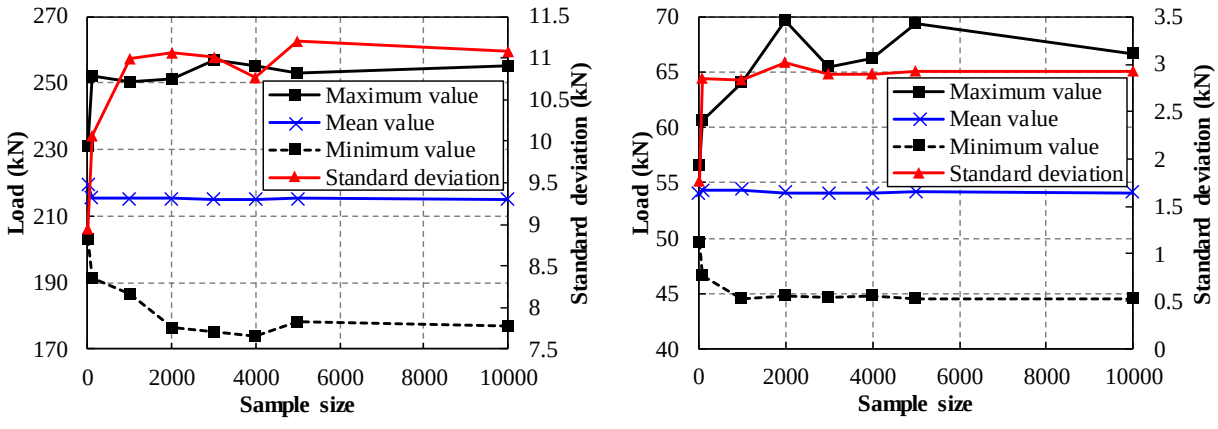

(a) P_w (b) P_v

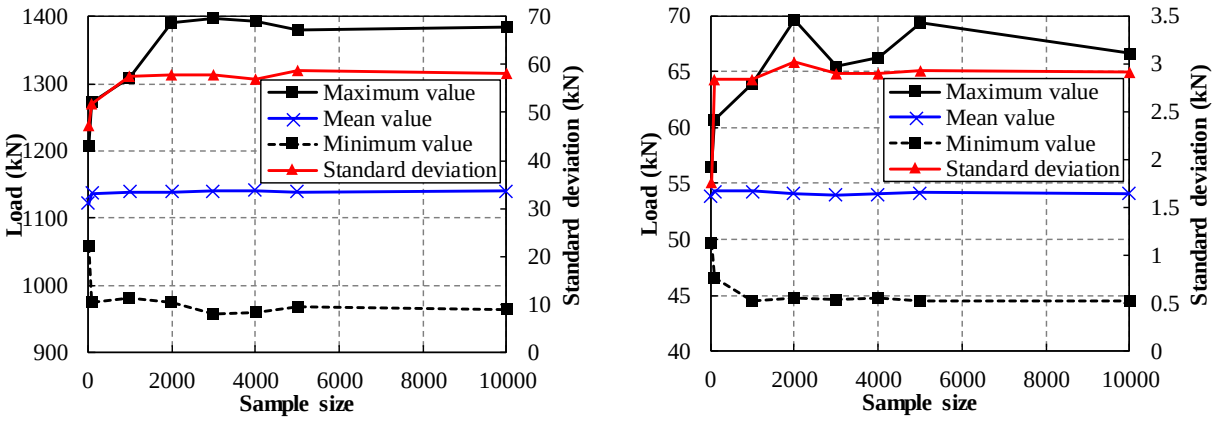

(c) P_r (d) P_{cr}

Fig. 6 Convergence study of Monte Carlo simulation

6.1. Sample size of Monte Carlo simulation

The steel angle member with the section of L100×100×12 and length of 4 m is selected to analyze the convergence of the Monte Carlo simulation. The section area loss ratio and corrosion depth are 50% and 9.6 mm (80% of the section thickness), respectively. The total number of corrosion pits in the section can be calculated by Equation (5), which is 125. Eight values of sample size are studied in the convergence analysis: 10, 100, 1000, 2000, 3000, 4000, 5000, and 10000. The results of buckling loads P_w, P_v, P_r, and P_{cr} in the convergence study are shown in Fig. 6. In these figures, the values of maximum, minimum, mean, and standard deviation of the buckling load for each sample size are presented. It can be seen that the sample size has a limited effect on the mean value of the buckling load of the member, while it has a relatively significant effect on the minimum, maximum, and standard deviation value of the buckling load. With the increase in the sample size, the minimum value of the buckling load decreases. The maximum and standard deviation values of the buckling load increase with the increase in the sample size. However, all the values tend to be stable when the sample size of the Monte Carlo simulation reaches 5000. Therefore, considering both the computational accuracy and cost, in the following study, the sample size of Monte Carlo simulation for a given area loss ratio and corrosion depth is designated to be 5000.

6.2. Buckling curve

Fig. 7 shows the lower bound of buckling curves of steel angle L200×100×12, in which Fig. 7(a) is for intact steel angle and Fig. 7(b)-(d) are for corroded steel angles with an area loss ratio of 50%. The legend name "$P_{crLowerB}$" refers to the lower bound of bifurcation buckling load P_{cr} of corroded steel angles. The corrosion depth for Fig. 7(b), Fig. 7(c) and Fig. 7(d) are 60%, 70%, and 80% of the section thickness, respectively. It can be seen from Fig. 7 that the bifurcation buckling load of the steel angle is always upper-bounded by the torsional buckling load P_r and flexural buckling load P_v. In Fig. 7(a), for the member length of 2 m, the flexural buckling load P_v is smaller than the torsional buckling load P_r, indicating that the buckling mode of the member is governed by the flexural buckling. In Fig. 7(b), however, for the member length of 2 m, the flexural buckling load P_v is greater than the torsional buckling load P_r, which suggests that the buckling mode of steel angle member will possibly be changed from flexural buckling to torsional buckling due to corrosion. Moreover, by comparing Fig. 7(b)-(d), it can be concluded that when the member length is small, even for a same area loss ratio, the bifurcation buckling load P_{cr} of steel angle can be significantly different due to the difference of corrosion depth. For example, in Fig. 7(b), for the member length of 0.5 m, the buckling load P_{cr} of steel angle with a corrosion depth of 60% is 320 kN, while it increases to 400 kN and 470 kN when the corrosion depth increases to 70% and 80%, respectively. However, with the increase in member length, the effect of corrosion depth on P_{cr} tends to decrease. For the member length of 2 m, the values of P_{cr} are all about 200 kN in Fig. 7(b)-(d). This is because when the member length increases, the bifurcation buckling load P_{cr} of the steel angle will be governed by the flexural buckling load, which is not significantly affected by the corrosion depth [16].

The lower bound of buckling curves of steel angle L150×100×12 is shown in Fig. 8. It can be observed from Fig. 7(b) and Fig. 8(b) that when the member length is relatively small, the bifurcation buckling load of steel angle L150×100×12 is greater than that of L200×100×12. This is because the section L200×100×12 is more asymmetric compared with section L150×100×12 and a more asymmetric section will result in a lower torsional buckling load of the steel angle. However, when the member length increases to more than 3 m, the bifurcation buckling load of the steel angle L150×100×12 becomes smaller than that of L200×100×12. Similar to Fig. 7, a change of the buckling mode of steel angle due to corrosion can also be observed in Fig. 8, *e.g.,* from Fig. 8(b) and Fig. 8(d), when the member length is 1.5 m, the buckling mode of the steel angle is governed by torsional buckling mode and flexural buckling mode, respectively.

To further quantify the effects of corrosion on the buckling loads of the steel angles, a reduction factor is defined, which is calculated by the ratio of the buckling load of the corroded steel angles to that of the intact steel angles. The reduction factors of the buckling loads of steel angle L200×100×12 and L150×100×12 with a length of 4 m are shown in Fig. 9(a) and Fig. 9(b), respectively. It is found that corrosion has the most detrimental effect on the torsional buckling load P_r of steel angles. When the area loss ratio reaches 50%, the buckling load P_{cr} and P_r of the steel angles decrease by more than 60% and 80%, respectively.

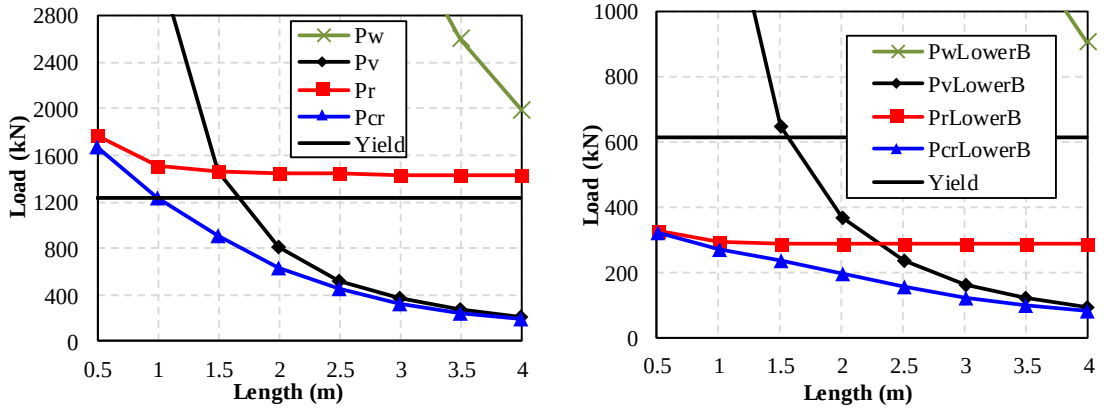

(a) Area loss ratio =0% and corrosion depth =0% (b) Area loss ratio =50% and corrosion depth =60%

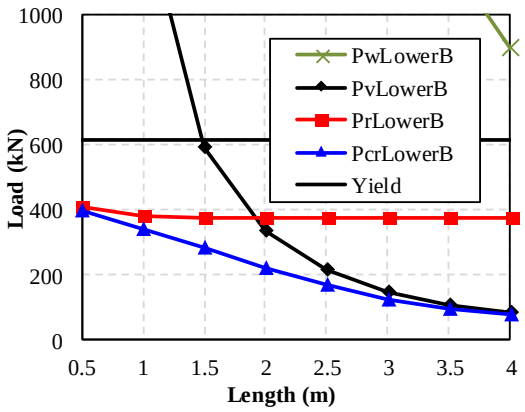

(c) Area loss ratio =50% and corrosion depth =70%

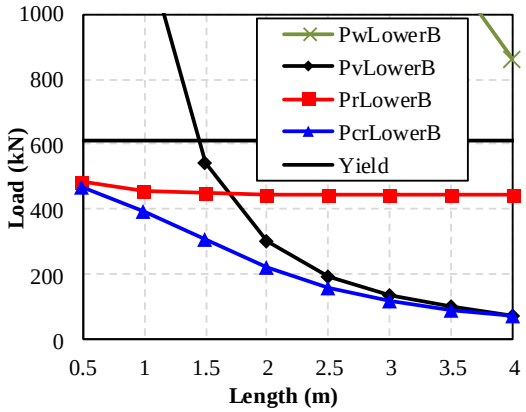

(d) Area loss ratio =50% and corrosion depth =80%

Fig. 7 Lower bound of buckling curve of steel angle L200×100×12

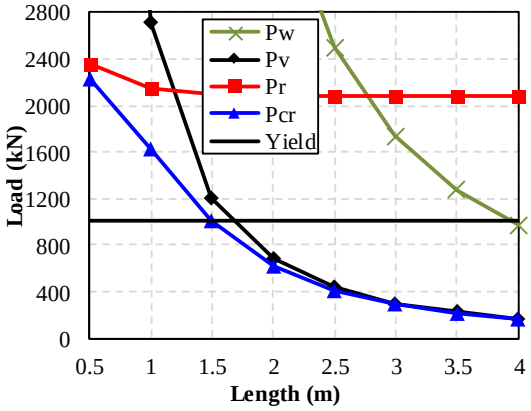

(a) Area loss ratio =0% and corrosion depth =0%

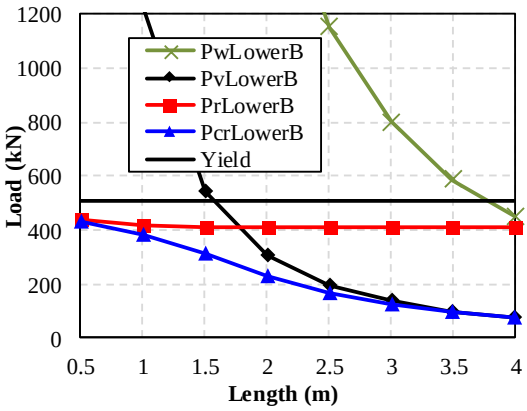

(b) Area loss ratio =50% and corrosion depth =60%

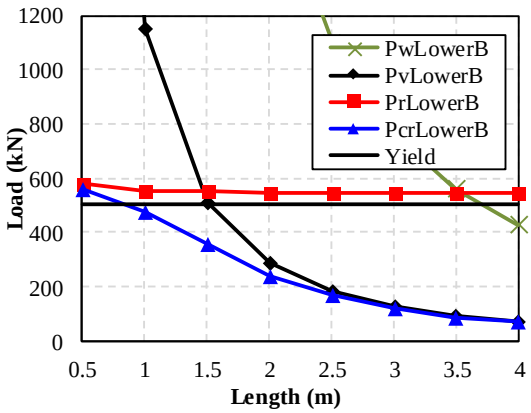

(c) Area loss ratio =50% and corrosion depth =70%

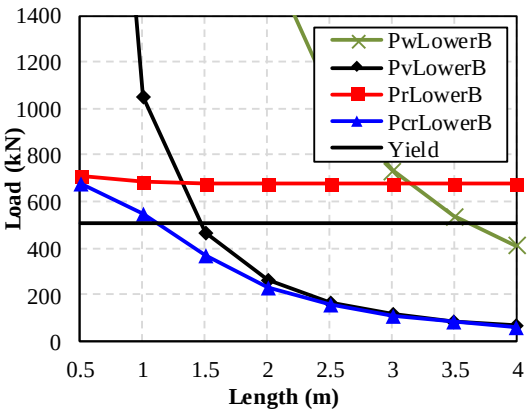

(d) Area loss ratio =50% and corrosion depth =80%

Fig. 8 Lower bound of buckling curve of steel angle L150×100×12

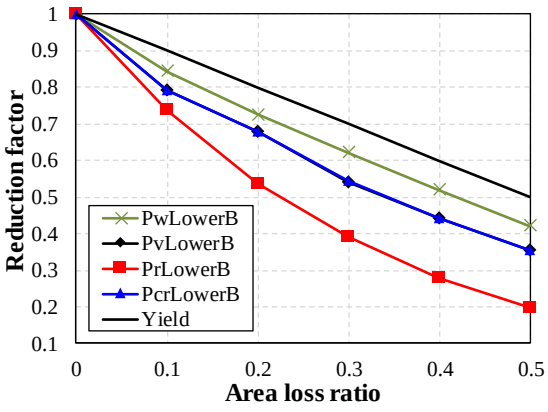

(a) L200×100×12

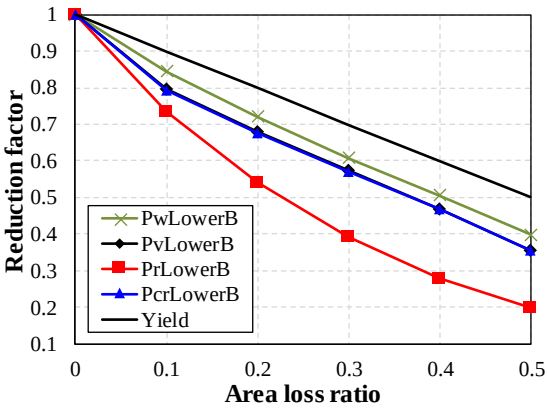

(b) L150×100×12

Fig. 9 Reduction factors of different buckling loads for member with length of 4 m

6.3. Effect of area loss ratio and corrosion depth

The effects of the area loss ratio on the bifurcation buckling load P_{cr} of steel angle L100×100×12 and L200×200×24 are shown in Fig. 10(a) and (b), respectively. The legend names "ALR" and "CD" refer to the section area loss ratio and corrosion depth, respectively. It has been found that a larger area loss ratio will result in a greater variation of the reduction factor. For instance, the reduction factor of the steel angle L100×100×12 ranges from 0.2-0.45 for the area loss ratio of 50%. However, the reduction factor ranges from 0.63 to 0.72 for the area loss ratio of 20%. When the member length increases, the reduction factor of buckling load P_{cr} tends to be a constant value. For the steel angle L100×100×12, when the member length is 4 m and corrosion depth is 60%, the reduction factor of the buckling load P_{cr} is about 0.72, 0.63, 0.52, and 0.46, corresponding to the area loss ratio of 20%, 30%, 40%, and 50%, respectively. The values of reduction factors for steel angle L200×200×24 in Fig. 10(b) are very close to those in Fig. 10(a).

The effects of corrosion depth on the buckling load P_{cr} of steel angle L100×100×12 and L200×200×24 are shown in Fig. 11(a) and (b), respectively. It is found that a smaller corrosion depth ratio will result in a greater variation of the reduction factor. For instance, the reduction factor of steel angle L100×100×12 ranges from 0.2-0.45 for the corrosion depth of 50%. However, the reduction factor ranges from 0.35-0.4 for the corrosion depth of 90%. It is interesting to note that a smaller corrosion depth will result in a smaller reduction factor for the member length of 0.5 m, but a larger reduction factor for the member length of 4 m. This phenomenon can also be discovered in Fig. 7 and Fig. 8. For the steel angle L100×100×12, when the member length is 4 m, and the area loss ratio is 50%, the reduction factor of the buckling load P_{cr} is about 0.45, 0.43, 0.42, and 0.4, corresponding to the corrosion depth of 60%, 70%, 80%, and 90%, respectively. The values of reduction factors for steel angle L200×200×24 in Fig. 11 (b) are very close to those in Fig. 11 (a)

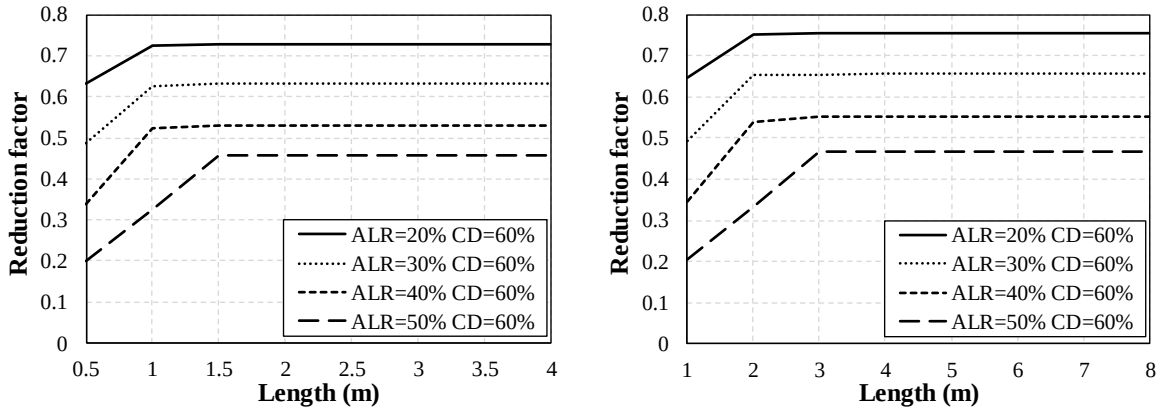

(a) L100×100×12 (b) L200×200×24

Fig. 10 Effect of area loss ratio on lower bound of buckling load P_{cr}

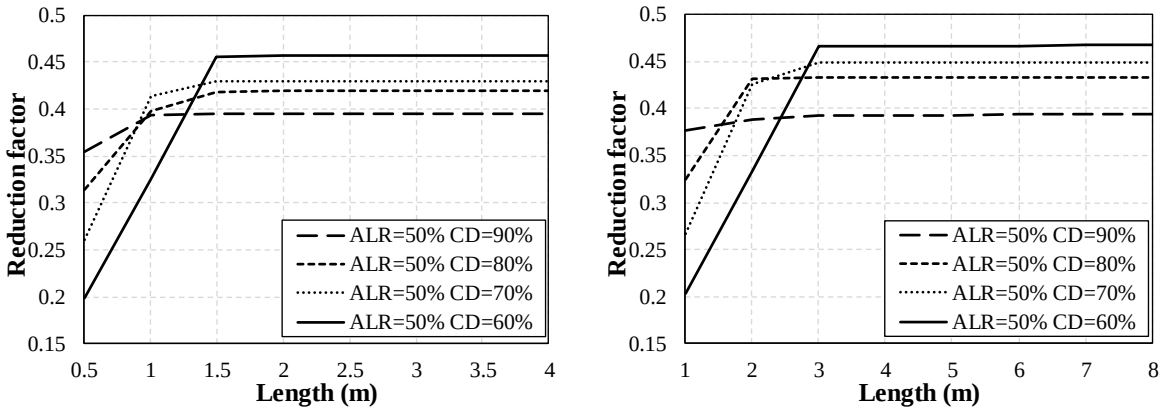

(a) L100×100×12 (b) L200×200×24

Fig. 11 Effect of corrosion depth on lower bound of buckling load P_{cr}

6.4. Discussion on the reduction factor

In Sections 6.2 and 6.3, only the lower bounds of the reduction factor of buckling load for steel angles are analyzed. To further study the corrosion effects on the buckling loads of steel angles, some key statistical characteristics, such as the mean value, standard deviation, and distribution of the reduction factors of buckling load P_{cr} from each Monte Carlo simulation are calculated. A probabilistic relationship between the reduction factor and area loss ratio is also established. The mean value and standard deviation of the reduction factor are shown in Table 3. Note that the total number of Monte Carlo simulations for a certain area loss ratio has considered the variations of corrosion depth. For example, for the area loss ratio of 10%, the possible corrosion depth can be 0.2t, 0.3t, 0.4t, 0.5t, 0.6t, 0.7t, 0.8t, and 0.9t (shown in Table 1). For each corrosion depth, the sample size of the Monte Carlo simulation is 5,000. Therefore, the total number of the Monte Carlo simulations for the area loss ratio of 10% is 40,000.

It can be seen that the mean values of the reduction factors of steel angles are about 0.9, 0.8, 0.7, 0.6, and 0.5 for the area loss ratio of 0.1, 0.2, 0.3, 0.4, and 0.5, respectively. The section type has a limited effect on the mean values of the reduction factors. However, the standard deviations of the reduction factors are affected by the section type. The section with larger asymmetry has a greater standard deviation of reduction factors. For example, for the area loss ratio of 50%, the standard deviation of reduction factors of steel angle L200×100×12 is 0.031, while the standard deviation of reduction factors of steel angle L200×200×24 is 0.0171. Moreover, a larger area loss ratio will also result in a larger standard deviation of reduction factors.

The probability density functions (PDFs) of the reduction factor for different steel angles are shown in Fig. 12. Take Fig. 12(a) as an example, the PDF is obtained as follows. For the area loss ratio of 10%, there are 40,000 values of reduction factors of the buckling load P_{cr}. The minimum value, maximum value, and range of these reduction factors are firstly determined. Then the range of reduction factors are divided into 25 intervals. For each interval, the number of reduction factors within this interval is determined, and the PDF can be calculated. For other area loss ratios, the PDF can be obtained in a similar way.

From the shape of the PDF for the reduction factors of buckling load P_{cr}, it can be found that the reduction factors generally obey a normal distribution. With the increase in area loss ratio, the shape of the PDF becomes wider and

shorter, indicating a greater standard deviation of the reduction factor. Fig. 13 compares the actual PDF and the PDF of normal distribution for the reduction factors of steel angle L100×100×12. Note that the PDF of reduction factors following the normal distribution can be determined once the actual mean value and standard deviation are known. The mean value and standard deviation of the reduction factors of buckling load P_{cr} for each steel angle are summarized in Table 3. It can be concluded from Fig. 13 that the normal distribution can reliably capture the characteristic of the distribution of the reduction factors.

Table 3
Mean value and standard deviation of the reduction factor of buckling load P_{cr}

Section	Area loss ratio	Total number of Monte Carlo simulation	Mean value μ	Standard deviation σ
L100×100×12	0.1	40,000	0.9019	0.0139
	0.2	35,000	0.8016	0.0189
	0.3	30,000	0.7029	0.0221
	0.4	25,000	0.6018	0.0239
	0.5	20,000	0.5029	0.0251
L150×150×18	0.1	40,000	0.9005	0.0114
	0.2	35,000	0.8005	0.0153
	0.3	30,000	0.7019	0.0178
	0.4	25,000	0.6009	0.0194
	0.5	20,000	0.502	0.0199
L200×200×24	0.1	40,000	0.9006	0.0098
	0.2	35,000	0.8007	0.0132
	0.3	30,000	0.7015	0.0152
	0.4	25,000	0.6011	0.0164
	0.5	20,000	0.5014	0.0171
L150×100×12	0.1	40,000	0.8992	0.0161
	0.2	35,000	0.7973	0.0218
	0.3	30,000	0.6964	0.0248
	0.4	25,000	0.5941	0.0264
	0.5	20,000	0.4939	0.0271
L200×100×12	0.1	40,000	0.895	0.0179
	0.2	35,000	0.7903	0.0242
	0.3	30,000	0.6875	0.0283
	0.4	25,000	0.583	0.0307
	0.5	20,000	0.4814	0.031

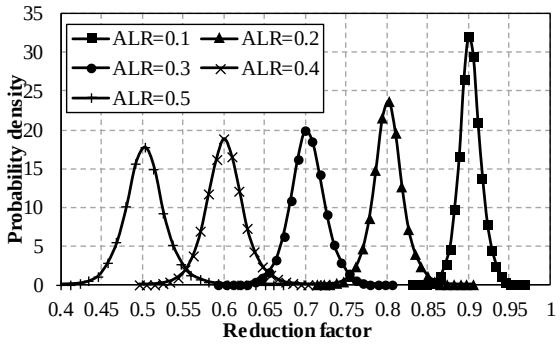

(a) L100×100×12

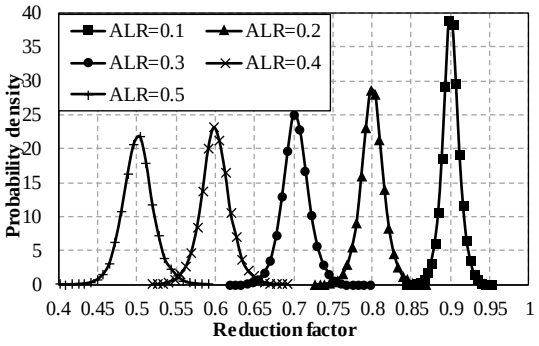

(b) L150×150×18

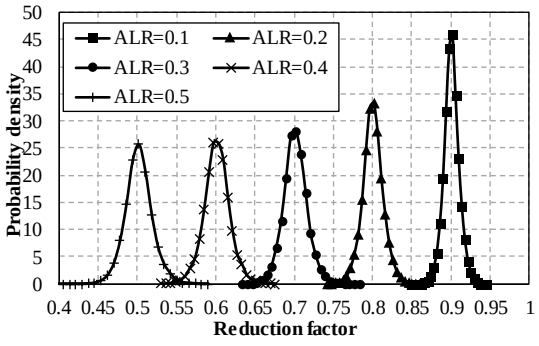

(c) L200×200×24

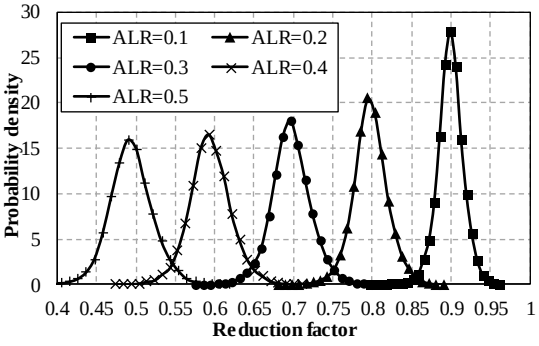

(d) L150×100×12

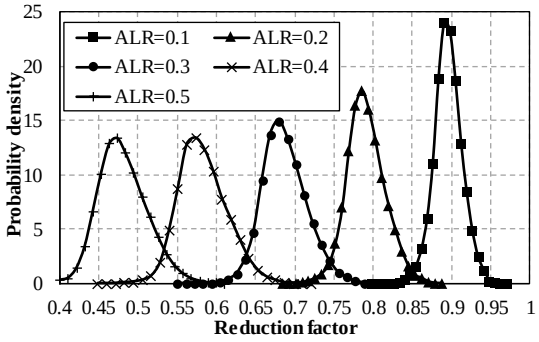

(e) L200×100×12

Fig. 12 Distribution of the reduction factor of buckling load P_{cr}

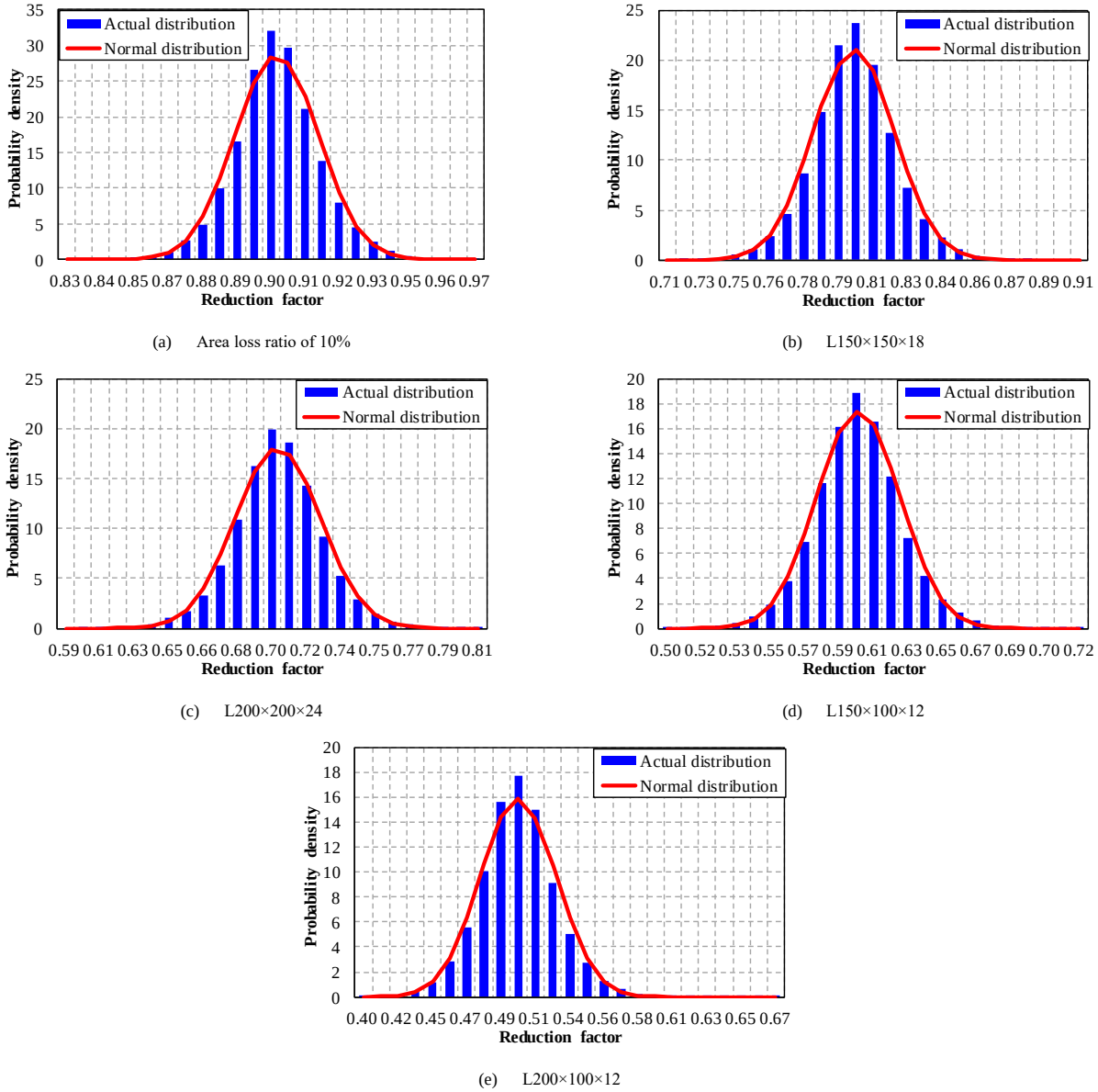

(a) Area loss ratio of 10%

(b) L150×150×18

(c) L200×200×24

(d) L150×100×12

(e) L200×100×12

Fig. 13 Goodness of fit test of the reduction factor for steel angle L100×100×12

6.5. Practical design method

Based on the results of parametric studies, a probabilistic relationship between the reduction factor of buckling load and area loss ratio for steel angle is established, as shown in Fig. 14. Note that the reduction factors for all steel angles are included in Fig. 14. Therefore, for area loss ratios of 0.1, 0.2, 0.3, 0.4, and 0.5, there are 200000, 175000, 150000, 125000, and 100000 dots shown in Fig. 14, respectively. The solid blue line indicates the mean value of the reduction factor. The dashed red line and solid red line are the lower bound and upper bound for the values within one standard deviation of the mean value, respectively. The dashed black line and solid black line are the lower bound and upper bound for the values within three times the standard deviation of the mean value, respectively.

Fig. 14 also gives the probability for the reduction factor within one, two, and three times the standard deviation of the mean value. For the area loss ratio of 0.1, the probabilities for the reduction factor within one, two, and three times the standard deviation of mean value are 0.725, 0.945, and 0.991, respectively, which are very close to the analytical values of 0.683, 0.955, and 0.997 for

normal distribution. It again indicates that the reduction factors of the buckling load of steel angles follow a normal distribution. It should be noted that the probability is calculated by the ratio of dot number satisfying requirements to the total dot number, rather than the ratio of segment length. For example, for the area loss ratio of 0.2, the probability for the reduction factor within three times the standard deviation of the mean value is 0.9913. However, the ratio of segment length within three times the standard deviation of mean value to total segment length is obviously less than 0.9913. This is because the distribution density of data fails to be shown in Fig. 14 due to the excessive amount of data.

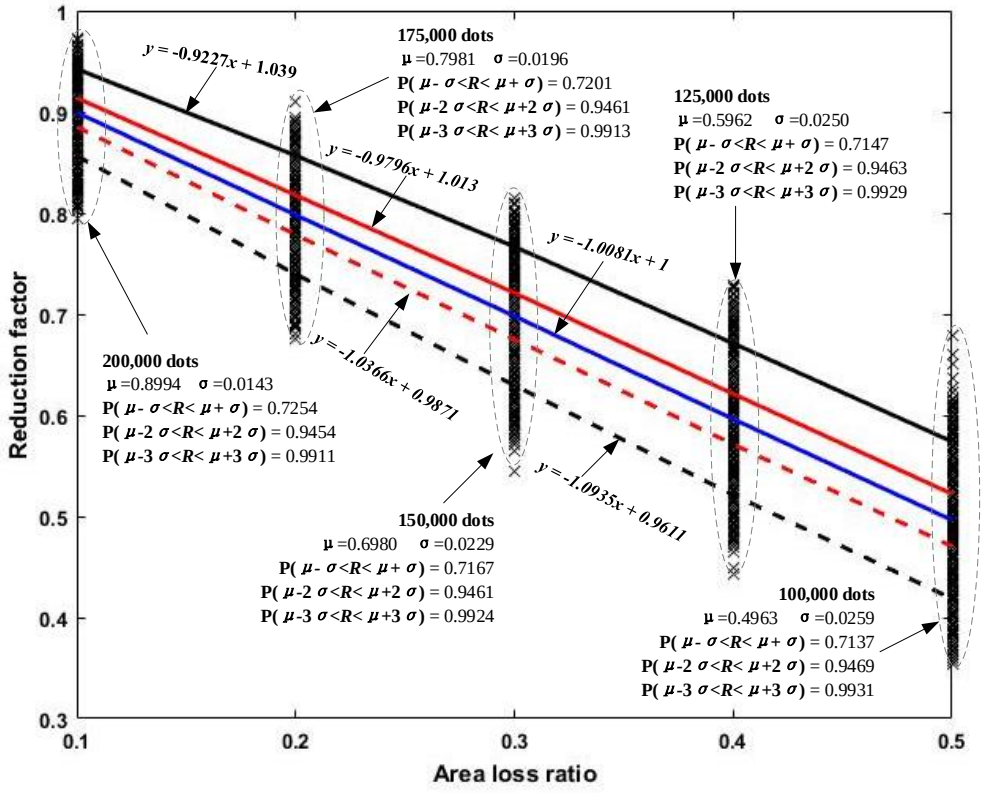

Fig. 14 Regression of the reduction factor of buckling load P_{cr} for all steel angle members

7. Conclusion

This paper presents a numerical study on the bifurcation buckling load of steel angle members with random corrosion pits. The effects of member length, section type, area loss ratio, and corrosion depth on the bifurcation buckling load of steel angles are studied. A probability-based relationship between the reduction factor of buckling load and the area loss ratio of steel angles is proposed. The following conclusions can be drawn from this study:

- The reduction factors of the buckling load of steel angles obey a normal distribution. A larger area loss ratio will result in a larger standard deviation of the reduction factors.
- For steel angles with the same area loss ratio, the mean values of the reduction factors of different section types are very close. For area loss ratios of 10%, 20%, 30%, 40%, and 50%, the mean values of the reduction factors of buckling load for steel angles are about 0.9, 0.8, 0.7, 0.6, and 0.5, respectively.
- The detrimental effects of corrosion on the torsional buckling load and flexural buckling load are different. Therefore, the buckling mode of steel angle members may changed from flexural buckling to torsional buckling due to corrosion.
- When the member length is small, the bifurcation buckling load of the steel angle is significantly affected by the corrosion depth. However, as the member length increases, the effect of corrosion depth tends to decrease.

References

[1] Kumar R, Cline DBH, Gardoni P. A stochastic framework to model deterioration in engineering systems. STRUCT SAF 2015;53:36-43.
[2] Zhao Z, Zhang H, Xian L, Liu H. Tensile strength of Q345 steel with random pitting corrosion based on numerical analysis. THIN WALL STRUCT 2020;148:106579.
[3] Xiao L, Peng J, Zhang J, Cai C. Mechanical Properties of Corroded High Performance Steel Specimens Based on 3D Scanning. ADV STEEL CONSTR 2019;15(2):129-36.
[4] Sheng J, Xia J. Effect of simulated pitting corrosion on the tensile properties of steel. CONSTR BUILD MATER 2017;131:90-100.
[5] Dang H, Liang A, Feng R, Zhang J, Yu X, Shao Y. Experimental study on mechanical properties and low-cycle fatigue behaviour of stainless steels subjected to salt spray and dry/wet cycle. INT J FATIGUE 2022;165:107187.
[6] Zhao Z, Zhang N, Wu J, Gao Y, Sun Q. Shear capacity of steel plates with random local corrosion. CONSTR BUILD MATER 2020;239:117816.
[7] Xu S, Qiu B. Experimental study on fatigue behavior of corroded steel. Materials Science and Engineering: A 2013;584:163-9.
[8] Silva JE, Garbatov Y, Guedes Soares C. Ultimate strength assessment of rectangular steel plates subjected to a random localised corrosion degradation. ENG STRUCT 2013;52:295-305.
[9] Wang R, Ajit Shenoi R, Sobey A. Ultimate strength assessment of plated steel structures with random pitting corrosion damage. J CONSTR STEEL RES 2018;143:331-42.
[10] Hua J, Wang F, Wang N, Huang L, Hai L, Li Y, et al. Experimental and numerical investigations on corroded stainless-clad bimetallic steel bar with artificial damage. J BUILD ENG 2021;44:102779.
[11] Zhang W, Chen J, Yu Q, Gu X. Corrosion evolution of steel bars in RC structures based on Markov chain modeling. STRUCT SAF 2021;88:102037.
[12] Ma Y, Guo Z, Wang L, Zhang J. Experimental investigation of corrosion effect on bond behavior between reinforcing bar and concrete. CONSTR BUILD MATER 2017;152:240-9.
[13] Srivaranun S, Akiyama M, Bocchini P, Christou V, Frangopol DM, Fukushima H, et al. Effect of the interaction of corrosion pits among multiple tensile rebars on the reliability of RC structures: Experimental and numerical investigation. STRUCT SAF 2021;93:102115.
[14] Liu J, Huang H, Ma ZJ, Chen J. Effect of shear reinforcement corrosion on interface shear transfer between concretes cast at different times. ENG STRUCT 2021;232:111872.
[15] Zhang Z, Xu S, Wang H, Nie B, Su C. Flexural buckling behavior of corroded hot-rolled H-section steel beams. ENG STRUCT 2021;229:111614.
[16] Chen L, Liu S, Zhang J, Yam MCH. Efficient algorithm for elastic buckling of corroded I-section steel members with Monte Carlo simulation. THIN WALL STRUCT 2022;175:109216.
[17] Zhao Z, Mo S, Xiong Q, Liu H, Liang B. Moment capacity of H-section steel beam with randomly located pitting corrosion. PROBABILIST ENG MECH 2021;66:103161.
[18] Zhang Z, Xu S, Wang Y, Nie B, Wei T. Local and post-buckling behavior of corroded axially-compressed steel columns. THIN WALL STRUCT 2020;157:107108.
[19] Wang R, Guo H, Shenoi RA. Experimental and numerical study of localized pitting effect on compressive behavior of tubular members. MAR STRUCT 2020;72:102784.
[20] Wang H, Zhang Z, Qian H, Fan F. Effect of local corrosion on the axial compression behavior of circular steel tubes. ENG STRUCT 2020;224.
[21] Wang R, Guo H, Shenoi RA. Compressive strength of tubular members with localized pitting damage considering variation of corrosion features. MAR STRUCT 2020;73:102805.
[22] Xu S, Zhang Z, Qin G. Study on the seismic performance of corroded H-shaped steel columns. ENG STRUCT 2019;191:39-61.
[23] Zhang J, Chen L, Liu S, Yam MCH. Efficient elastic buckling assessment algorithm for steel members with random non-uniform corrosion. ENG STRUCT 2022;266:114550.
[24] Hisazumi K, Kanno R. Column Buckling of Corroded Steel Angles and Channels: Experiments and Failure Mode Analyses. J STRUCT ENG 2021;147(8).
[25] Zhao Z, Zhou S, Zheng C, Tang L. Predictions of compression capacity of randomly corroded

WHSJs based on artificial neural network. MECH ADV MATER STRUC 2020:1-9.
[26] Yang Y, Li W, Xu T, He Z, Zhao D. Experimental study of hysteretic behavior of corroded steel with multi-angle welding joints. J CONSTR STEEL RES 2021;187:106990.
[27] Wang H, Wang Y, Zhang Z, Liu X, Xu S. Cyclic behavior and hysteresis model of beam-column joint under salt spray corrosion environment. J CONSTR STEEL RES 2021;183:106737.
[28] Chen H, Liu H, Chen Z. Residual behaviour of corroded welded hollow spherical joints subjected to eccentric loads. J CONSTR STEEL RES 2021;182:106661.
[29] Bao J, Zhou W. A random field model of external metal-loss corrosion on buried pipelines. STRUCT SAF 2021;91:102095.
[30] Chakraborty S, Tesfamariam S. Subset simulation based approach for space-time-dependent system reliability analysis of corroding pipelines. STRUCT SAF 2021;90:102073.
[31] Mazumder RK, Salman AM, Li Y. Failure risk analysis of pipelines using data-driven machine learning algorithms. STRUCT SAF 2021;89:102047.
[32] Bu Y, Yang L, Zhu Z, Wang F. Testing, simulation and design of offshore lined pipes under axial compression. MAR STRUCT 2022;82:103147.
[33] Zhang X, Zheng S, Zhao X. Experimental and numerical study on seismic performance of corroded steel frames in chloride environment. J CONSTR STEEL RES 2020;171:106164.
[34] Yang Y, Wu Q, He Z, Jia Z, Zhang X. Seismic Collapse Performance of Jacket Offshore Platforms with Time-Variant Zonal Corrosion Model. APPL OCEAN RES 2019;84:268-78.
[35] Ji CY, Xue HZ, Shi XH, Gaidai O. Experimental and numerical study on collapse of aged jacket platforms caused by corrosion or fatigue cracking. ENG STRUCT 2016;112:14-22.
[36] Zhang H, Ha L, Li Q, Beer M. Imprecise probability analysis of steel structures subject to atmospheric corrosion. STRUCT SAF 2017;67:62-9.
[37] Huang W, Garbatov Y, Guedes Soares C. Fatigue reliability of a web frame subjected to random non-uniform corrosion wastage. STRUCT SAF 2014;48:51-62.
[38] OSZVALD K. Buckling of Corroded Steel Angle Members under Compression.; 2014.
[39] Zhang L, Liang Y, Zhao O. Laboratory testing and numerical modelling of pin-ended hot-rolled stainless steel angle section columns failing by flexural-torsional buckling. THIN WALL STRUCT 2021;161:107395.
[40] Ziemian RD. Guide to Stability Design Criteria for Metal Structures: John Wiley & Sons, 2010.
[41] Liu S, Gao W, Ziemian RD. Improved line-element formulations for the stability analysis of arbitrarily-shaped open-section beam-columns. THIN WALL STRUCT 2019;144:106290.
[42] R. Ziemian, W. McGuire, S.W. Liu. MASTAN2 v4.0.; 2019.
[43] The British Standards Institution. Structural Steel Equal and Unequal Leg Angles (BS EN 10056-1:2017).; 2018.